This article has been accepted for publication in a future issue of this journal, but has not been fully edited. Content may change prior to final publication. Citation information: DOI 10.1109/TMAG.2015.2446414, IEEE Transactions on Magnetics

Harmonic Analysis of Low Stator Slot and Rotor Pole Combination FSPM Machine Topology for High Speed

Dheeraj Bobba[1], *Student Member, IEEE,* Yingjie Li[1], *Student Member, IEEE,* and Bulent Sarlioglu[1], *Senior Member, IEEE*

[1] University of Wisconsin-Madison
Wisconsin Electric Machines and Power Electronic Consortium (WEMPEC), Madison, WI 53706 USA

The high speed machine design is becoming important due to advantages such as high power density and small size. Flux switching permanent magnet (FSPM) machines have a simple rotor design without any windings or permanent magnets which makes them apt for high speed operation. A low pole topology of FSPM machine is desirable to keep the operational frequency to a minimum. The lowest slot-pole combination for a three phase FSPM machine is the 6 stator slot 4 rotor pole topology. This research aims to investigate and analyze the cause of the unbalance in the flux linkage and back EMF waveforms of such FSPM machine. The influence of rotor pole width, stator tooth width, and the magnet length have been analyzed to find the optimum design variable. Results will be useful in making this low pole FSPM topology amenable for high speed operation.

Index Terms **− Flux switching machine, high speed, harmonic analysis, low pole, permanent magnet.**

I. Introduction

APPLICATIONS with weight and size restrictions, such as industrial, aerospace, and transportation have high specific power as an important requirement. In recent years, permanent magnet (PM) synchronous machines are often used for such applications due to high energy density permanent magnets. Flux switching permanent magnet (FSPM) machines, which belong to the family of PM synchronous machines, are known to produce higher torque densities compared to traditional PM topologies [1] - [3] However, significantly less attention has converged towards low-slot pole machines such as the proposed 6 stator slot 4 rotor pole (6/4) combination.

Due to the simple rotor construction with magnets and armature winding incorporated on the stator, it can be inferred that FSPM machine topology is suitable for high speed applications. However, the fundamental frequency required for an FSPM machine is dependent on the number of rotor poles and generally much higher compared to traditional PM machines. This results in higher losses in core and power electronics. Demanding switching frequencies limit the speeds at which FSPM machines can be viable. Much of the available literature is focused on high slot pole combination of FSPM machines [4] - [6] since low slot pole combinations were found to produce unbalanced flux linkages [7], [8]. In order to reduce the fundamental frequency, the number of rotor poles must be minimized.

In this paper, research results that are geared toward the attainments of high speed capability of 6/4 FSPM topology are presented. One of the main contributions of the paper is to discover and explain the cause of the second harmonic in the flux linkage waveform of 6/4 FSPM configuration. A parametric analysis is performed to measure the influence of the stator and rotor pole width and identify the optimum design parameters to minimize the unbalance. The design parameters are then fed to an optimization algorithm based on the second order response surface method [9], [10]. The objectives include increasing the fundamental flux linkage component and reducing the second order flux linkage, thus reducing the overall material costs.

TABLE I
PARAMETERS FOR 6/4 FSPM MACHINE

Parameter	Value
Rated Speed (RPM)	15000
Stator Outer Diameter (mm)	112.3
Stator Inner Diameter (mm)	73
Air gap (mm)	1
Magnet Width (mm)	9.6
Stack Length (mm)	63.2
Phase Resistance (mΩ)	15
Number of Turns per Coil	10
Coils per Phase	2

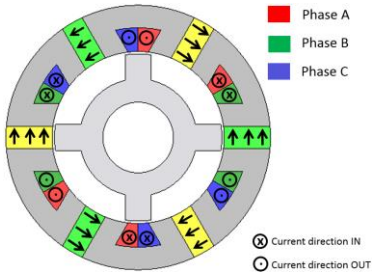

Fig. 1. FEA model for 6/4 FSPM machine.

II. Harmonic Analysis

A 6/4 FSPM topology is the lowest possible slot pole FSPM combination for a three phase machine and operates with lowest fundamental frequency for any given speed, hence it is amenable for high speed. The equations shown in [11] can be used to predict that 6/4 topology produces unbalanced back EMF. Multiple combinations were evaluated and experimentally verified in [8], [12]. By similarity, various stator and rotor pole combinations were sized and analyzed in [7] along with a 6/4 topology and it verified the prediction that the flux linkage and back EMF waveforms are unbalanced in nature. Such a 6/4 FSPM machine is reconstructed as a 2D model using FEA software as shown in Fig. 1. Steady state analysis is performed for the open circuit case with the rotor spinning at 15,000 RPM. The dimensions and parameters used in the simulation are shown in Table I

The flux linkage and back EMF waveforms that were obtained from FEA are shown in Fig. 2 and Fig. 3, respectively.

This article has been accepted for publication in a future issue of this journal, but has not been fully edited. Content may change prior to final publication. Citation information: DOI 10.1109/TMAG.2015.2446414, IEEE Transactions on Magnetics

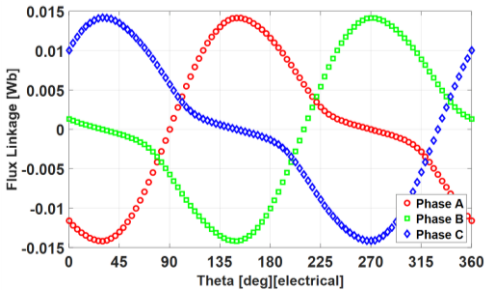

Fig. 2 - Flux linkage waveform from FEA for 6/4 FSPM topology.

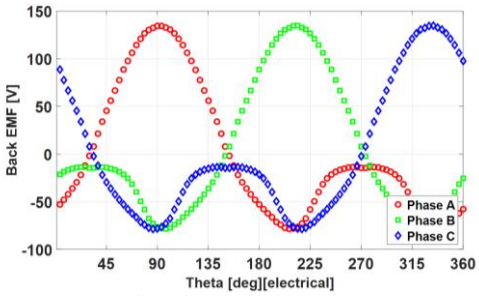

Fig. 3. Back EMF waveform from FEA for 6/4 topology.

It can be seen that the back EMF waveform is distorted and the flux linkage waveform is also nonsinusoidal.

The FFT was applied to the flux linkage waveform and the resultant harmonic magnitudes and phases are plotted in Fig. 4. It can be seen that there is a dominant 2nd order harmonic present. Also, it is observed that the higher order harmonics have an insignificant magnitude relative to fundamental and second order harmonic components. Neglecting the higher order terms, a Fourier expression of the flux linkage waveform of phase *A* can be written as:

$$\lambda_A = \sum_{h=1}^{2} \lambda_{A_h} \cos(h\omega t + \theta_{A_h}), \quad (1)$$

where h is the harmonic component, ω is the fundamental frequency in radians per second, and θ is the phase angle in radians for corresponding harmonic components.

The magnitudes and phases used in the equation for phase *A* are as shown in Table II. It can be noted that the second order component has a phase difference of 90° with respect to the fundamental. However, this phase difference cannot be used to cancel out the second order component because, 6 slot topologies lack the second set of phase shifted stator windings as in the case of 12 slot topology.

Similarly, the flux linkage equations for phases *B* and *C* can be written as:

$$\lambda_B = \sum_{h=1}^{2} \lambda_{B_h} \cos(h\omega t + 2\pi/3 + \theta_{B_h}), \quad (2)$$

$$\lambda_C = \sum_{h=1}^{2} \lambda_{C_h} \cos(h\omega t - 2\pi/3 + \theta_{C_h}). \quad (3)$$

The expression for back EMF for phase *A* can now be written as,

$$e_a = \sum_{h=1}^{2} h\omega\lambda_{A_h} \sin(h\omega t + \theta_{A_h}). \quad (4)$$

Individual fundamental and second order components of flux linkage and their summation are plotted in Fig. 5. The resultant flux linkage is compared to the original waveforms obtained from FEA in Fig. 6. It should be noted that FEA results include all harmonics while harmonic sum given by (1) comprises of

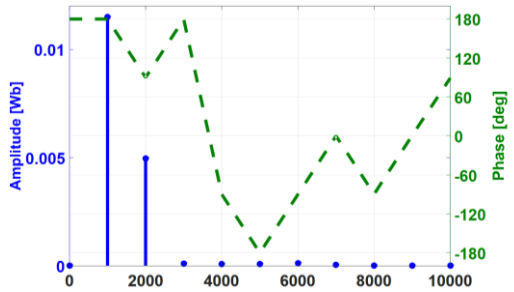

Fig. 4. FFT of flux linkage of Phase *A*.

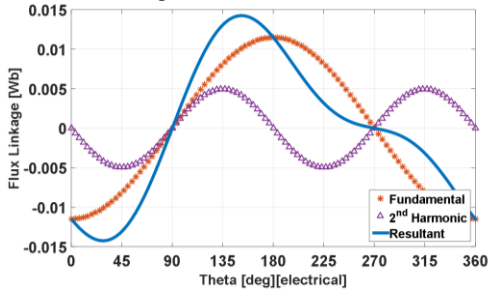

Fig. 5. Summation of first two harmonics of flux linkage for Phase *A*.

TABLE II.
FFT CONSTANTS FOR PHASE *A*

h	*f[Hz]*	λ_{A_h}*[Wb]*	θ_{A_h}*[rad]*
0	*0*	*0*	π
1	*1000*	*0.01149628*	π
2	*2000*	*0.00495859*	$\pi/2$

only fundamental and second order components. The comparison between FEA and harmonic sum verifies that accuracy is not lost in neglecting higher order harmonic components in harmonic sum.

This analysis identifies that a dominant second order component is causing the distortion in the resultant waveforms. Back EMF from the harmonic sum is also compared with FEA as shown in Fig. 7. There is a small deviation due to the neglected higher order harmonics. While the higher order components have negligible magnitudes for flux linkage, they have a slightly higher contribution in back EMF. This is due to the factor $h\omega$ multiplied to corresponding h^{th} harmonic magnitude. However, because the second order is the dominant component, if it can be reduced or eliminated, the response will be more sinusoidal.

Further investigation was conducted to understand the cause of second order harmonic component. The fundamental and second order harmonic components are plotted and the rotor positions noted against the peaks and zero points on the waveforms over one cycle. The waveforms and their respective rotor positions with magnetic flux density vectors are shown in Fig. 8 and Fig. 9. The 'go' and 'return' paths of Phase *A* are marked on the coils.

It can be observed that the duration of the second order waveform, Fig. 9(a) to Fig. 9(e), is equal to the duration of the d-axis of rotor pole sweeping across the stator tooth width. The negative peak is occurring when the rotor pole d-axis is at the beginning of magnet position as in Fig. 9(b) and positive peak when the rotor d-axis is at the end of magnet position as in Fig. 9(d). The fundamental component period is equal to the

This article has been accepted for publication in a future issue of this journal, but has not been fully edited. Content may change prior to final publication. Citation information: DOI 10.1109/TMAG.2015.2446414, IEEE Transactions on Magnetics

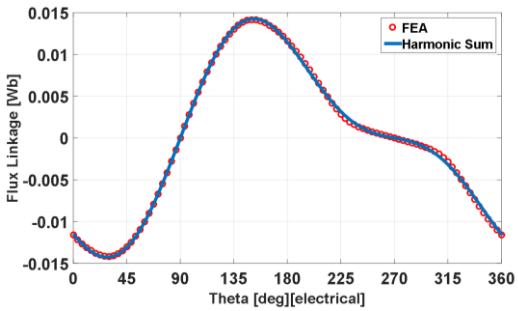

Fig. 6. FEA flux linkage and harmonic sum comparison.

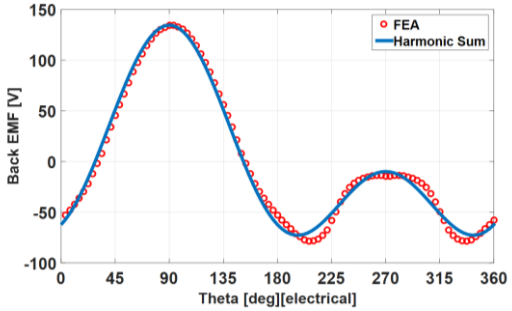

Fig. 7. FEA back EMF and harmonic sum comparison.

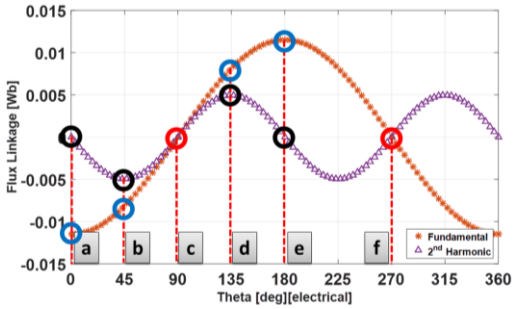

Fig. 8. Fundamental and second order components of phase *A*.

duration of the rotor pole d-axis sweeping across the adjacent stator tooth before phase *A* coil carrying current in the negative direction to the adjacent tooth after phase *A* coil carrying current in the positive direction.

From these figures, it is clear that the second harmonic is a resultant of the uneven permeance distribution across the air gap as the rotor pole sweeps across the stator tooth width. If the distribution of permeance can be made more uniform, the second order harmonic may be reduced or eliminated.

III. Influence of Geometry on Harmonics

A parametric analysis was conducted by varying the widths of the stator tooth and the rotor pole to measure the influence of the widths on the magnitudes of individual harmonic components. The width of the magnet was not changed to keep the source flux constant while verifying the influence of teeth width on the flux linkage. Since the variation may change the peak flux linkage as well as the magnitude of the fundamental component, a harmonic ratio term is introduced to compare the influence. It is defined as:

$$Harmonic\ Ratio = \left(\left| \lambda_{A_2} \right| / \left| \lambda_{A_1} \right| \right) k_s , \qquad (5)$$

where $|\lambda_{A_1}|$ is the magnitude of the fundamental component of flux linkage, $|\lambda_{A_2}|$ is the magnitude of the second order

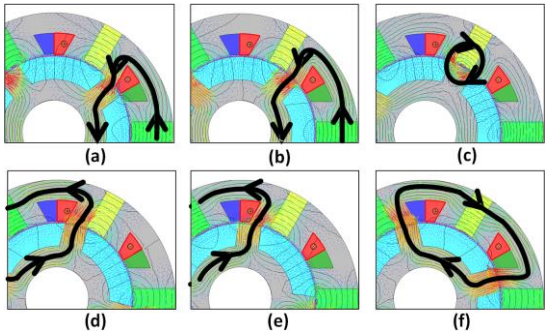

Fig. 9. Rotor positions with respect to the fundamental and second harmonic component values.

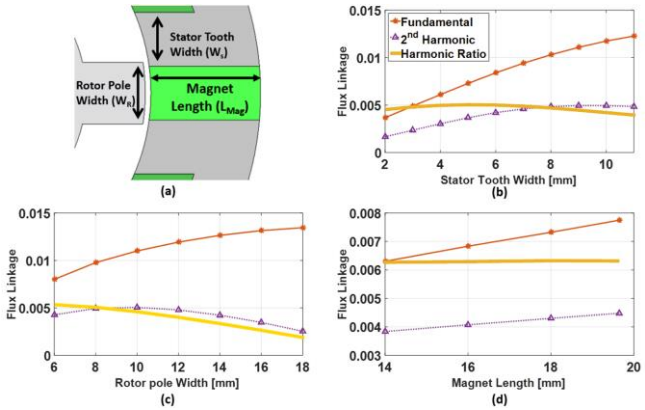

Fig. 10. Parametric analysis (a) Parameters in geometry (b) Results for stator tooth width, (c) Results for rotor pole width, (d) Results for magnet length.

component of flux linkage and k_s is a scaling factor used to make the harmonic ratio magnitude comparable with the flux linkage amplitude and the value is chosen based on the amplitude of fundamental component. As the harmonic ratio increases, the dominance of the second order component increases, thereby increasing the distortion in flux linkage. Therefore, a smaller harmonic ratio is desired.

The stator tooth width (W_S) is varied from 2 mm to 11 mm and the rotor pole width (W_R) is varied from 6 mm to 18 mm. Also, having a slightly reduced magnet length reduces the eddy currents in the magnets [13]. Such reduction may be required for any modification of the stator pole shape. The magnet length (L_{Mag}) is also varied from 14 mm to 19.5 mm. The geometric parameters are as shown in Fig. 10(a). The amplitudes of individual harmonic components and the scaled harmonic ratio are plotted in Fig. 10(b) to Fig. 10(d) for stator tooth variation, rotor pole variation and magnet length variation, respectively. The scaling factor (k_s) for the harmonic ratio plotted was chosen as 10^{-2}.

We observed that the harmonic ratio has a distinctive peak with the variation of the stator tooth width and rotor pole width, but the harmonic ratio for magnet length is mostly linear. This indicates that both fundamental and second harmonic components are equally influenced. Furthermore, we observed that the peak occurs when the dimensions of the rotor pole and stator tooth are equal. Based on this analysis, having a higher rotor pole to stator tooth width ratio is advantageous in reducing the second order harmonic component. Whereas, a higher stator tooth to rotor pole width ratio also shows a similar behavior. There are fewer restrictions with increasing the rotor pole width

This article has been accepted for publication in a future issue of this journal, but has not been fully edited. Content may change prior to final publication. Citation information: DOI 10.1109/TMAG.2015.2446414, IEEE Transactions on Magnetics

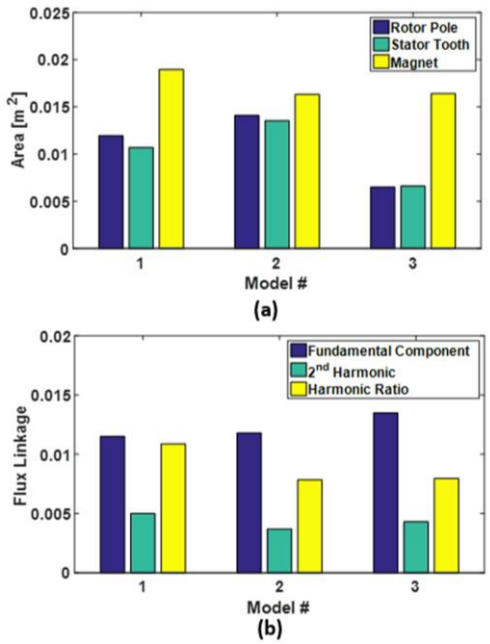

Fig. 11. Optimization analysis comparison for selected cases (a) Cross section area (b) Flux linkage and harmonic ratio.

compared to stator tooth width. As seen in Fig. 10(c), the harmonic ratio is reduced by almost 50% when the stator tooth width is held at 10 mm and the rotor pole width is increased to 18 mm.

A multivariable optimization is performed using a second order response surface algorithm to identify the optimum combination of the geometric parameters such that the fundamental component of flux density is increased and the second order harmonic component is reduced. The cost function is defined as,

$$f_c(x) = w_1 A_{pole} + w_2 A_{tooth} + w_3 A_{mag}, \qquad (6)$$

where w_1, w_2, and w_3 are the weight functions assigned according to the material costs. A_{pole}, A_{tooth}, and A_{mag} represent the cross section area of rotor pole, stator tooth, and magnet, respectively. Because the magnet dimensions have a significant impact on the overall costs, the cross section area of magnet carries a higher weight. The initial design is labeled as Model 1. Two best designs are selected from the optimization results such that Model 2 represents the lowest second harmonic component and Model 3 represents the lowest cost function. The cross section areas of rotor pole, stator tooth, and magnet are plotted in Fig. 11(a) and fundamental flux linkage, second order flux linkage, and harmonic ratio are plotted in Fig. 11(b).

As part of cost versus performance improvement, a relatively higher fundamental component can be seen in Model 3 at a lower material cost. Alternatively the second order component can be reduced at the expense of more material cost.

IV. Conclusion

This paper contributes to the improvement of flux linkage waveform of the 6/4 FSPM topology and make it suitable for high speed operation with minimum fundamental frequency. This will reduce the fundamental frequency required for any base speed by 60% compared to the existing widely studied 12/10 FSPM topology. The flux linkage waveform is decomposed using FFT and the reduced order harmonic equations are presented. The resulting plots are compared with FEA results to verify the influence of higher order harmonics.

A parametric analysis is performed to measure the influence of geometry on the harmonic component of flux linkage and identify the effective design parameters. It was identified that having equal pole and tooth width generates the highest amount of distortion and having a higher rotor pole to stator tooth ratio would reduce the harmonic magnitude as much as 50%. Optimization is performed to reduce the material volume and second harmonic component while boosting the fundamental component of flux linkage. It was identified that the flux linkage can be improved while the rotor pole and stator tooth material volume is reduced by 40% and magnet volume is reduced by 13%.

References

[1] Y. Pang, Z. Zhu, D. Howe, S. Iwasaki, R. Deodhar and A. Pride, "Comparative study of flux-switching and interior permanent magnet machines," in *Proc. ICEMS*, Oct. 2007.

[2] W. Hua, M. Cheng, Z. Zhu, W. Zhao and X. Kong, "Comparison of electromagnetic performance of brushless motors having magnets in stator and rotor," *Journal of Applied Physics*, vol. 103, no. 7, pp. 07F124-07F124,3, 2008.

[3] E. Sulaiman, T. Kosaka and N. Matsui, "High power density design of 6-slot–8-pole hybrid excitation flux switching machine for hybrid electric vehicles," *IEEE Trans. Magn.*, vol. 47, no. 10, pp. 4453-4456, Oct. 2011.

[4] W. Hua, M. Cheng, H. Jia and X. Fu., "Comparative study of flux-switching and doubly-salient PM machines particularly on torque capability," in *Proc. Industry Applications Society Annual Meeting*, Oct. 2008.

[5] W. Hua, M. Cheng and G. Zhang, "A novel hybrid excitation flux-switching motor for hybrid vehicles," *IEEE Trans. Magn.*, vol. 45, no. 10, pp. 4728-4731, Oct. 2009.

[6] M. Cheng, W. Hua, J. Zhang and W. Zhao, "Overview of stator-permanent magnet brushless machines," *IEEE Trans. Ind. Electron.*, vol. 58, no. 11, pp. 5087-5101, Nov. 2011.

[7] Y. Li, S. Li, Y. Yang and B. Sarlioglu, "Analysis of flux switching permanent magnet machine design for high-speed applications," in *Proc. of ECCE*, Sept. 2014.

[8] J. Chen and Z. Zhu, "Winding configurations and optimal stator and rotor pole combination of flux-switching PM brushless AC machines," *IEEE Trans. Energy Convers.*, vol. 25, no. 2, pp. 293-302, Nov. 2009.

[9] G. Lei, W. Xu, J. Hu, J. Zhu, Y. Guo and K. Shao, "Multilevel design optimization of a FSPMM drive system by using sequential subspace optimization method," *IEEE Trans. Magn.*, vol. 50, no. 2, pp. 685-688, Feb. 2014.

[10] X. Zhu, B. Yan, L. Chen, R. Zhang, L. Quan and L. Mo, "Multi-objective optimization design of a magnetic planetary geared permanent magnet brushless machine by combined design of experiments and response surface methods," *IEEE Trans. Magn.*, vol. 50, no. 11, pp. 1-4, Nov. 2014.

[11] J. Chen and Z. Zhu, "Comparison of all- and alternate-poles-wound flux-switching PM machines having different stator and rotor pole numbers," *IEEE Trans. Ind. Appl.*, vol. 46, no. 4, pp. 1406-1415, Sept. 2009.

[12] J. Chen and Z. Zhu, "Influence of the rotor pole number on optimal parameters in flux-switching PM brushless AC machines by the lumped-parameter magnetic circuit model," *IEEE Trans. Ind. Appl.*, vol. 46, no. 4, pp. 1381-1388, May 2010.

[13] Z. Zhu, Y. Pang, J. Chen, R. Owen, D. Howe, S. Iwasaki, R. Deodhar and A. Pride, "Analysis and reduction of magnet eddy current loss in flux-switching permanent magnet machines," in *Proc. IET Conference on Power Electronics, Machines and Drives*, April 2008.